Mon. Not. R. Astron. Soc. **000**, 1–12 (2013) Printed 10 September 2014 (MN LATEX style file v2.2)

The temperature dependence of the far-infrared–radio correlation in the *Herschel*-ATLAS⋆

D. J. B. Smith[1]†, M. J. Jarvis[2,3], M. J. Hardcastle[1], M. Vaccari[3], N. Bourne[4], L. Dunne[5], E. Ibar[6], N. Maddox[7], M. Prescott[3], C. Vlahakis[8], S. Eales[9], S. J. Maddox[5], M. W. L. Smith[9], E.Valiante[9], G. de Zotti[10,11]

[1]*Centre for Astrophysics, Science & Technology Research Institute, University of Hertfordshire, Hatfield, Herts, AL10 9AB*
[2]*Department of Astrophysics, Denys Wilkinson Building, Keble Road, Oxford, OX1 3RH*
[3]*Physics Department, University of the Western Cape, Private Bag X17, Bellville 7535, South Africa*
[4]*Institute for Astronomy, University of Edinburgh, Blackford Hill, Edinburgh EH9 3HJ*
[5]*Department of Physics and Astronomy, University of Canterbury, Private Bag 4800, Christchurch, 8140, New Zealand*
[6]*Instituto de Física y Astronomía, Universidad de Valparaíso, Avda. Gran Bretaña 1111, Valparaíso, Chile*
[7]*Department of Astronomy, University of Cape Town, Private Bag X3, Rondebosch 7701, South Africa*
[8]*Joint ALMA Observatory/European Southern Observatory, Alonso de Cordova 3107, Vitacura, Santiago, Chile*
[9]*School of Physics and Astronomy, Cardiff University, Queen's Buildings, The Parade, Cardiff, CF24 3AA*
[10]*INAF-Osservatorio Astronomico di Padova, Vicolo Osservatorio 5, I-35122 Padova, Italy*
[11]*SISSA, Via Bonomea 265, I-34136 Trieste, Italy*

10 September 2014

ABSTRACT

We use 10,387 galaxies from the *Herschel* Astrophysical TeraHertz Large Area Survey (*H*-ATLAS) to probe the far-infrared radio correlation (FIRC) of star forming galaxies as a function of redshift, wavelength, and effective dust temperature. All of the sources in our 250 μm-selected sample have spectroscopic redshifts, as well as 1.4 GHz flux density estimates measured from the Faint Images of the Radio Sky at Twenty centimetres (FIRST) survey. This enables us to study not only individual sources, but also the average properties of the 250 μm selected population using median stacking techniques. We find that individual sources detected at $\geq 5\sigma$ in both the *H*-ATLAS and FIRST data have logarithmic flux ratios (i.e. FIRC q_λ parameters) consistent with previous studies of the FIRC. In contrast, the stacked values show larger q_λ, suggesting excess far-IR flux density/luminosity in 250 μm selected sources above what has been seen in previous analyses. In addition, we find evidence that 250 μm sources with warm dust SEDs have a larger 1.4 GHz luminosity than the cooler sources in our sample. Though we find no evidence for redshift evolution of the monochromatic FIRC, our analysis reveals significant temperature dependence. Whilst the FIRC is reasonably constant with temperature at 100 μm, we find increasing inverse correlation with temperature as we probe longer PACS and SPIRE wavelengths. These results may have important implications for the use of monochromatic dust luminosity as a star formation rate indicator in star-forming galaxies, and in the future, for using radio data to determine galaxy star formation rates.

Key words: infrared: galaxies, ISM, radio continuum: galaxies

1 INTRODUCTION

Until recently, the most widely used samples of galaxies selected at far-infrared wavelengths in the local Universe have been derived from wide-field observations using the *Infra-Red Astronomical Satellite* (*IRAS*; Neugebauer et al. 1984). Since the *IRAS* catalogues (Helou & Walker 1988; Moshir et al. 1992; Wang & Rowan-Robinson 2009) are selected at 60 μm, sampling the Wien region of the far-infrared spectral energy distribution (SED), *IRAS*-derived samples typically comprise galaxies whose far-IR energy output is dominated by warm dust at temperatures of $30 - 60$ K. The vast increase in far-infrared sensitivity at longer wavelengths afforded by the *Herschel Space Observatory* (hereafter *Herschel;* Pilbratt et al. 2010) allied with its wide-field capabilities, have made it possible for the first time to select large samples of local galaxies at wavelengths $\lambda \gtrsim 100$ μm, where cool dust ($T \sim 10 - 30$ K) dominates the SED (e.g. Eales et al. 2010; Dunne et al. 2011).

The traditional model of the warm dust content of galaxies is that the far-IR emission is associated with the stellar birth clouds, with O- and B-type stars thought to dominate the dust heating (e.g. de Jong et al. 1984; Helou et al. 1985; Sauvage & Thuan 1992). Since the stars thought to be heating the dust are short-lived ($\sim 10 - 100$ Myr), the thermal far-infared emission has been widely used as a star formation rate indicator (Kennicutt 1998; Calzetti et al. 2010; Kennicutt & Evans 2012), with the integrated dust emission frequently estimated from sparsely-sampled photometry by assuming or deriving a model dust spectrum, as the observations permit.

⋆ *Herschel* is an ESA space observatory with science instruments provided by European-led Principal Investigator consortia and with important participation from NASA

† E-mail:daniel.j.b.smith@gmail.com(DS)

In the *Herschel* era, our understanding of the dust properties of galaxies is being transformed, partially through enabling us to select and study large samples of galaxies at longer far-IR wavelengths (e.g. Dunne et al. 2011; Smith et al. 2012). In particular, the unprecedented sensitivity of *Herschel*-SPIRE at 250 μm has highlighted the prevalence of cooler dust in normal star-forming galaxies (though this was by no means a new idea; see e.g. de Jong et al. 1984; Kennicutt 1998; Dunne et al. 2000; Dunne & Eales 2001; Vlahakis et al. 2005; Draine et al. 2007). This cool dust is thought to be associated with the diffuse interstellar medium (ISM), and to be heated by older stars with longer lifetimes than those which dominate the stellar birth clouds (e.g. Dale et al. 2012; Smith et al. 2012; Bendo et al. 2012); consequently, little correlation between the cold dust luminosity and recent star formation might be expected[1].

Though the most luminous radio sources are associated with non-thermal synchrotron emission from active galactic nuclei (hereafter AGN), at lower luminosities the source counts become dominated by star forming galaxies (e.g. Windhorst 2003; Wilman et al. 2008; Massardi et al. 2010; Wilman et al. 2010). In these sources, the relativistic electrons emitting the synchrotron radiation are thought to have been accelerated by shocks resulting from frequent supernovae, the end points of the same stars that inhabit the stellar birth clouds and heat the dust (energy which is then re-radiated in the far-infrared). These relativistic electrons are thought to persist in the magnetic field of a galaxy for a few tens of Myr emitting synchrotron radiation (e.g. Condon 1992). As a result, radio luminosity has also been frequently used as a star formation rate indicator (Condon 1992; Bell 2003).

It is therefore not surprising that the far-infrared emission of galaxies should show some relationship to the radio emission. What is surprising about this relationship – the far-infrared–radio correlation, hereafter FIRC – is that it is linear, that it shows remarkably little scatter, and that it persists both over several orders of magnitude in luminosity and for galaxies across the Hubble sequence (van der Kruit 1971; de Jong et al. 1985; Helou et al. 1985; Yun et al. 2001; Garrett 2002).

Several recent studies of the FIRC have investigated whether it evolves with redshift, using data from the *Spitzer Space Telescope* and comparatively small areal coverage at radio wavelengths in well-studied extra-galactic survey fields (e.g. Appleton et al. 2004; Frayer et al. 2006; Ibar et al. 2008; Murphy et al. 2009; Seymour et al. 2009; Michałowski et al. 2010; Sargent et al. 2010; Bourne et al. 2011) or for handfuls of sources using *BLAST* (Ivison et al. 2010a), *SCUBA* (Vlahakis et al. 2007), and *Herschel* (Ivison et al. 2010b). These studies show apparently contradictory results; Seymour et al. (2009) for example, found evidence for redshift evolution, whereas Appleton et al. (2004) did not. Though the observational evidence for an evolving FIRC is uncertain, it is possible that the apparently contradictory results discussed above might be reconciled with a non-evolving intrinsic FIRC, depending on the effects of different selection functions in the studies mentioned above (the aforementioned studies by Appleton et al. and Seymour et al. exemplify this, being selected at far-IR and radio wavelengths, respectively). For example evolution/uncertainty in the far-IR SEDs of high-redshift sources might lead to uncertain k-corrections (e.g. Bourne et al. 2011; Seymour et al. 2009), and there is also the possibility of contamination by low-luminosity AGN (e.g. Verma et al. 2002), especially for the higher-redshift studies (e.g. Sargent et al. 2010; Jarvis et al. 2010).

There are many possible scenarios in which one might expect to observe an evolving FIRC (see Lacki et al. 2010; Lacki & Thompson 2010, for details). One reason might be variations in the typical magnetic field strength in galaxies (which would influence the radio emission but is unlikely to affect the thermal dust emission). Another possible source of FIRC evolution could be changing dust temperatures (e.g. due to the strong temperature dependence of luminosity for modified black body radiation, coupled with k-correction effects), or changes in the dust distribution within a galaxy.

In what follows we build on the results of Jarvis et al. (2010) to revisit the empirical properties of the FIRC at low redshift, taking particular interest in the possible influence of the effective dust temperature. We do this by taking advantage of the order of magnitude increase in the area covered by the latest release of the *Herschel* Astrophysical TeraHertz Large Area Survey (hereafter *H*-ATLAS), and the presence of shorter wavelength *H*-ATLAS data at 100 and 160 μm, which were unavailable at the time of the previous study. The presence of these data is particularly crucial for our investigation, since a recent study by Smith et al. (2013) highlighted their importance for determining isothermal dust temperatures for local galaxies.

In section 2 we describe the data used and our sample selection, while in section 3 we describe our methods of calculating the radio and far-infrared effective temperatures/luminosities along with the FIRC. We present our results in section 4 and make some concluding remarks in section 5. We assume a standard ΛCDM cosmology with $H_0 = 71\,\mathrm{km\,s^{-1}\,Mpc^{-1}}$, $\Omega_M = 0.27$ and $\Omega_\Lambda = 0.73$ throughout.

2 OBSERVATIONS

2.1 *Herschel*-ATLAS data

This study is based on observations made with the *Herschel Space Observatory* as part of the *Herschel*-ATLAS survey (Eales et al. 2010, Valiante et al., *in prep*). The *H*-ATLAS catalogue consists of broad-band photometric imaging at 100 and 160 μm from the PACS instrument (Poglitsch et al. 2010), and at 250, 350 and 500 μm from the SPIRE instrument (Griffin et al. 2010), covering $\sim$161 deg^2 over the three equatorial fields from the Galaxy And Mass Assembly (GAMA) survey (Driver et al. 2011); further details of the GAMA survey selection and strategy can be found in Baldry et al. (2010) and Robotham et al. (2010). Details of the *H*-ATLAS map-making, source extraction and catalogue generation can be found in Ibar et al. (2010); Pascale et al. (2011); Rigby et al. (2011) and Maddox et al., *in prep*. For this analysis, we use the far-IR flux densities in each of the PACS/SPIRE bands taken from the current *H*-ATLAS catalogue; the 5σ point source limits for each band in order of increasing wavelength are 130, 130, 30.4, 36.9 & 40.1 mJy, including confusion noise, with beam size between 9 and 35 arcsec FWHM.

The current *H*-ATLAS catalogue recommends including calibration uncertainties of 10 per cent of the measured flux density for the PACS bands, and 7 per cent for the SPIRE bands, which we add in quadrature to the estimated errors on the catalogue photometry. The *H*-ATLAS catalogue has been cross-identified with r-band

[1] Though in some cases stellar birth clouds may not be totally optically thick, and can "leak" UV photons; there may still be some correlation between heating of the diffuse ISM and recent star formation (see e.g. Popescu et al. 2002).

sources in the Sloan Digital Sky Survey (SDSS; York et al. 2000), using the likelihood ratio technique discussed in Smith et al. (2011, see also Bourne et al. *in prep*).

In this study, we include $> 5\sigma$ 250 μm sources with reliable ($R > 0.80$) optical counterparts, and robust spectroscopic redshifts from GAMA in the latest *H*-ATLAS catalogue, which contains 13,084 sources which meet these criteria at $z < 0.5$ (though see section 2.2 below for a discussion of resolved sources).

2.2 Radio data

We use radio observations from the June 2013 release of the Faint Images of the Radio Sky at Twenty-cm survey (hereafter FIRST; Becker et al. 1995), which covers 10,000 deg^2 of the Northern Sky at 1.4 GHz, with a typical RMS sensitivity of 0.15 mJy beam^{-1} in the fields overlapping *H*-ATLAS. The *H*-ATLAS fields are also covered by the NRAO VLA Sky Survey (hereafter NVSS; Condon et al. 1998) with 45 arc sec resolution and sensitivity of 0.45 mJy beam^{-1}, and there is also coverage of roughly half of the *H*-ATLAS area at 325 MHz taken using the Giant Metre-wave Radio Telescope (Mauch et al. 2013), though the sensitivity varies considerably.

In what follows we intend not only to probe the FIRC for individual galaxies that are well detected at 1.4 GHz, but also to statistically probe the FIRC for the 250 μm-selected population as a whole. Therefore we do not use existing flux-density limited catalogues but instead follow Jarvis et al. (2010), and use the FIRST and NVSS imaging data directly, producing cutout images 5 arcmin on a side centred on the optical positions associated to our 250 μm sources.

We used the cutout images to perform aperture photometry on the FIRST maps, using 5 arc sec radius circular apertures centred on the positions of the reliable SDSS counterparts to the 250 μm sources. We derived uncertainties on each measurement by reading off the value from the FIRST RMS maps, downloaded from the project website[2], and accounting for the size of the aperture (i.e. converting from Jy beam^{-1} to Jy aperture^{-1}). To check that this rescaling was correct, we systematically offset each aperture by 1 arcminute in a random direction, and made a histogram of the resulting extracted aperture fluxes, which were found to be consistent with the expected Gaussian distribution. The FIRST flux densities derived in this way gave excellent agreement (i.e. residuals consistent with the expected distribution once the uncertainties are taken in to account) with the values for the detected sources included in the June 2013 version of the FIRST catalogue.

The potential advantage of the low resolution of NVSS relative to FIRST (i.e. possible greater resistance to resolved radio sources in our analysis; Jarvis et al. 2010), is offset by the lower sensitivity (i.e. lower signal-to-noise in the stacks, and fewer individual source detections), and by the fact that the NVSS images are quantized in increments of 0.1 mJy (which is comparable to the average 1.4 GHz flux density of an *H*-ATLAS 250 μm source; see section 4.2). In addition, reproducing the NVSS catalogue fluxes for even the unresolved sources in our sample requires corrections for fitting, confusion and *additive* clean biases (Condon et al. 1998), with the latter bias being particularly difficult to apply to stacked flux densities.

We also conducted a comparison between our FIRST aperture flux densities and the NVSS catalogue values for the 78 sources with have $\geq 5\sigma$ detections in each of the 250 μm catalogue, our FIRST aperture flux densities, and the NVSS catalogue (i.e. 250um sources with NVSS catalogue flux densities > 2.1 mJy). The comparison reveals that the two sets of values are consistent (i.e. the residuals are again consistent with the expected distribution given the uncertainties).[3] This indicates that interferometer resolution effects (e.g. missing large scale diffuse emission in the FIRST maps) are not an issue for our sample. With these concerns in mind, we use our own FIRST aperture flux densities directly measured from the cutout images in what follows.

3 METHOD

3.1 Far-IR SED fitting

3.1.1 Isothermal SED fits

Our sample consists of sources with $> 5\sigma$ 250 μm detections (including confusion noise) with reliable optical counterparts and spectroscopic redshifts. In order to derive the simplest possible temperature estimates for our sample, we assume a single-component modified blackbody model of the standard form:

$$f_\nu \propto \frac{\nu^{3+\beta}}{\exp\left(\frac{h\nu}{kT}\right) - 1}, \quad (1)$$

where h is the Planck constant, k is the Boltzmann constant, and T represents the dust temperature. The additional term β (known as the emissivity index) modifies the traditional Planck function by assuming that the dust emissivity varies as a power law of frequency, ν^β. Following Smith et al. (2013), we assume a fixed β of 1.82 (similar to the value derived by e.g. Planck Collaboration et al. 2011), and compare the five bands of *H*-ATLAS photometry for each source with a grid of isothermal models with temperatures between 5 and 60 K, accounting for the transmission through the *Herschel* response curves. The temperature of the isothermal model can be a useful empirical measure of the effective temperature of a galaxy's dust SED (Smith et al. 2013).

By recording the values of χ^2 for every galaxy at every temperature on the grid, we are able to build a marginalized probability distribution function (hereafter PDF) for the effective temperature of each object, $T_{\rm eff}$. We use our PDFs to generate median likelihood estimates of $T_{\rm eff}$ for each galaxy (we use median-likelihood temperatures rather than best-fit estimates since Smith et al. 2013, showed that they are less susceptible to bias when using *H*-ATLAS data to estimate them, though the difference is small[4]), with un-

[2] http://sundog.stsci.edu/

[3] We note that a subset of sixteen sources have a significant NVSS flux excess; upon visual inspection of the SDSS, FIRST and NVSS images for these sources, it becomes clear that in nine cases the NVSS excess is a result of blending with an unrelated nearby source in the large NVSS beam, while six are clearly double-lobed structures, and are recognised as AGN using our $q_{250} < 1.2$ criterion discussed in section 4. The remaining source with an NVSS flux excess is also flagged as an AGN by our q_{250} criterion, though unlike the previous six sources, this is not evident from its radio morphology. This offers further encouragement for our implementation of the Hardcastle et al. (2013) method of identifying AGN.

[4] The small differences between the median-likelihood and best-fit estimates of $T_{\rm eff}$ are shown in figure 14 of Smith et al. (2013), which contains simulations showing that the median-likelihood estimates have slightly narrower probability density contours than the best-fits (i.e. they are recovered more precisely), and that they exhibit better behaviour near the bounds of the temperature prior.

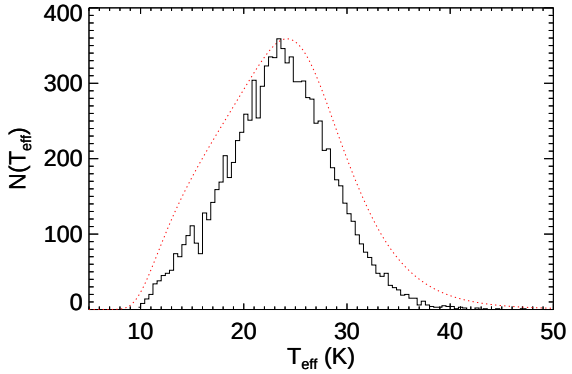

Figure 1. The effective temperatures recovered for our sample based on the isothermal SED fitting; median likelihood values are shown as the histogram (in black) and are overlaid with the summed temperature PDF for our sample (red dotted line) renormalised to have the same peak value as the histogram. The vast majority are in the range $10 < T_{\rm eff} < 40\,{\rm K}$ despite fitting with a temperature prior distribution that is flat between $5 < T < 60\,{\rm K}$.

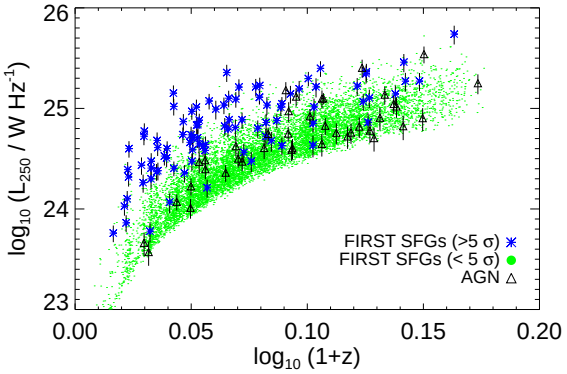

Figure 2. Relationship between redshift and 250 μm monochromatic luminosity, L_{250}, for galaxies where the radio emission is dominated by star formation according to FIRST (blue asterisks), by AGN (black triangles) and the 250 μm galaxy population that is not detected by FIRST (in green). The AGN have been identified using a method analogous to that of Hardcastle et al. (2013); see text for more details.

certainties derived from the $16^{\rm th}$ and $84^{\rm th}$ percentiles of the temperature PDF. To highlight the range of temperatures that we find for galaxies in our sample, figure 1 shows a histogram of the median likelihood temperature estimates recovered for our sample (in black), overlaid with the sum of each individual temperature PDF (in red; which can give some indication of the uncertainties on the median likelihood values).

Smith et al. (2013) used simulations designed to closely match the *H*-ATLAS data set (including realistic models of both the instrumental and confusion noise in each band) to determine how well effective temperatures can be estimated for *H*-ATLAS sources. Using a superset of the galaxies that we study here, Smith et al. (2013) found that unbiased temperature estimates could be determined provided that PACS data were included in the SED fitting, irrespective of whether a particular source is formally detected by PACS or not (to e.g. 3σ). Since the *H*-ATLAS catalogue (like the simulations in Smith et al. 2013) contains flux density estimates in each band irrespective of their formal significance, we use the catalogue values as maximum likelihood estimates, and consequently we do not have to use upper limits in our fitting. Using the results of Smith et al. (2013) we find that the average uncertainty in $T_{\rm eff}$ is $\Delta T_{\rm eff}/T_{\rm eff} \approx 0.166$ across the full range of temperatures recovered here (figure 1), ranging from $\Delta T_{\rm eff} \sim 2\,{\rm K}$ at 10K to $\Delta T_{\rm eff} \approx 6\,{\rm K}$ at 40 K.

3.1.2 Estimating Integrated dust luminosities

Dust in galaxies is not isothermal; though the dust SED generally peaks at $\lambda \gtrsim 80\,\mu$m, there is also a varying contribution to the integrated dust luminosity from very small, hot grains that are bright in the mid-infrared (e.g. Yang et al. 2007), and this contribution can exceed 0.3 dex in luminosity. Though the *H*-ATLAS fields are covered by mid-infrared data from the Wide-field Infrared Survey Explorer (WISE; Wright et al. 2010), and extensive efforts have been made to provide aperture-matched WISE photometry for *H*-ATLAS sources (Cluver et al. 2014), the preliminary catalogues contain detections in the W4 (22 μm) band for < 5 per cent of our sample. As a result, the vast majority of our integrated dust luminosities are strongly model-dependent, limited in precision due to the variable contribution of the mid-infrared to the integrated luminosity, and subject to possible bias that is difficult to quantify (see appendix A for more details).

For these reasons, we do not use integrated dust luminosities in our analysis. However, our simplest isothermal estimates of $L_{\rm dust}$ (integrated between 3-1000 μm) show that the majority of our sample have far-infrared luminosities in the star-forming galaxy regime, with $10.0 < \log_{10}(L_{\rm dust}/L_{\odot}) < 11.0$, though there is a substantial minority in the luminous infrared galaxy category; $\log_{10}(L_{\rm dust}/L_{\odot}) > 11.0$ (see also Smith et al. 2013).

3.1.3 Estimating FIR monochromatic luminosities

Whilst the integrated dust luminosities for our sample show dependence on the choice of SED template used, our monochromatic luminosity estimates are much more robust. This is a result of the high-quality *H*-ATLAS far-IR photometry (i.e. the data are uniform, and the photometric scatter is small), and the generally precise k-corrections (k_{λ}) that we are able to derive for our $z < 0.5$ sample. To determine k_{λ} we require a best estimate of the underlying dust SED; for this task we use the best-fit SED for each galaxy from the Siebenmorgen & Krügel (2007, hereafter SK07) model library. We use SK07 SEDs because they are able to recover good fits to the *H*-ATLAS data across the full range of effective temperatures shown in figure 1, and because they are more realistic than the isothermal models.

The accuracy of our k_{λ} is discussed in appendix A, but to summarise, the median uncertainty on the individual k-corrections ranges from ~ 14 per cent at 250 μm to ~ 25 per cent at 100 μm, though the uncertainty on k_{100} at the coldest temperatures is rather larger. In what follows we account for the uncertainty on k_{λ} by adding the estimated errors in quadrature with the uncertainties on the individual flux densities taken from the *H*-ATLAS catalogue. The monochromatic L_{250} for galaxies in our sample as a function of redshift are shown in figure 2.

3.2 Calculating 1.4 GHz luminosity

Since we use FIRST aperture flux densities in our analysis for the reasons discussed in section 2.2, we minimize the influence of resolved sources on our studies of the FIRC by excluding all sources

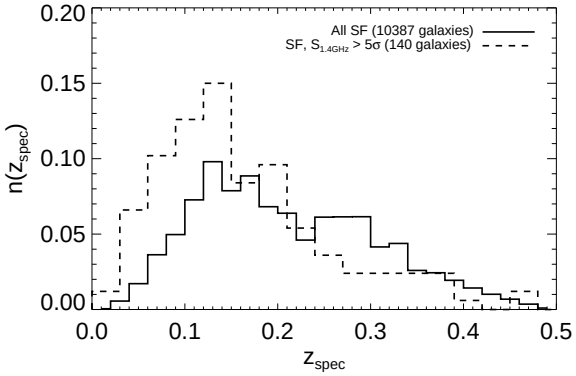

Figure 3. The redshift distribution of the 10,387 250 μm selected *H*-ATLAS sample with spectroscopic redshifts $z_{spec} < 0.5$ (solid lines) and isophotal major axes < 10 arc sec. Also overlaid (dashed line) is the redshift distribution of the subset of 140 galaxies which have $> 5\sigma$ detections at 1.4 GHz in FIRST; see section 3.2 for details.

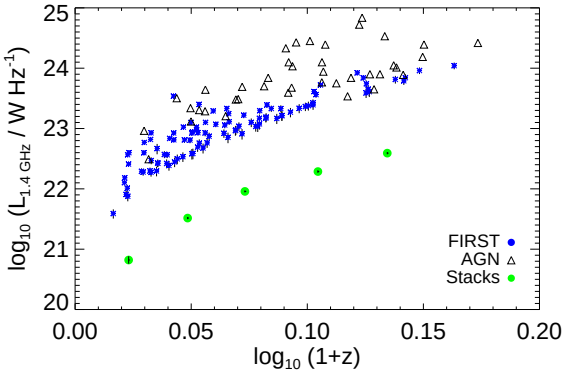

Figure 4. The 1.4 GHz luminosity density of sources in our sample as a function of redshift, with those sources in the starburst regime detected by FIRST shown in blue. The median stacked 1.4 GHz luminosity density for all 250 μm sources in our sample, divided between five bins of redshift are shown as the green circles. Sources with a substantial AGN contribution to $L_{1.4\,\mathrm{GHz}}$ are shown as black triangles; see section 4 for details of their identification.

with SDSS major axes > 10 arc sec. We k-correct the 1.4 GHz luminosity density to the rest frame for each source by assuming spectral indices which are randomly drawn from a Gaussian distribution centred about $\alpha = 0.71$ with an RMS of 0.38 (using the convention that $S_\nu \propto \nu^{-\alpha}$; Condon 1992). These values for α were derived by Mauch et al. (2013) using 90 deg^2 of 325 MHz and 1.4 GHz data within the *H*-ATLAS fields. Since the sources in this study are all at $z < 0.5$, the derived k-corrections are small (the median uncertainty on this k-correction for our sample is ~ 6.3 per cent), however we account for this additional source of uncertainty in two ways. Firstly, we repeated our analyses 100 times using random draws from the Gaussian α distribution, finding that our results are unchanged within the errors. Secondly, we propagate our estimates of the uncertainty on each individual k-correction (derived by determining the standard deviation of $k_{1.4\mathrm{GHz}}$ as a function of redshift) through to the derived luminosities by adding them in quadrature with the uncertainties on the 1.4 GHz flux density estimates themselves.

The spectroscopic redshift distributions of 250 μm sources with $\geq 5\sigma$ 1.4 GHz detections, and all 250 μm detected sources in our sample are shown in figure 3, with both distributions peaking at $z_{\mathrm{spec}} \approx 0.13$. In figure 4 we show $L_{1.4\,\mathrm{GHz}}$ as a function of redshift, with the 250 μm selected star-forming galaxies with SNR > 5 at 1.4 GHz shown in blue, and the stacked values for our whole 250 μm sample in bins of redshift shown in green. The stacked values are obtained by simply taking the median of the individual $L_{1.4\,\mathrm{GHz}}$ values (whether statistically significant or not) in bins at intervals of 0.03 in $\log_{10}(1+z)$, except for the highest-z bin which contains all sources at $\log_{10} z_{spec} > 0.012$.

3.3 Calculating the far-infrared–radio correlation

The dimensionless parameter describing the FIRC, q, is defined as the logarithmic ratio of the far-infrared luminosity L_{dust}, integrated between 3-1000 μm in the rest-frame, to the rest-frame 1.4 GHz k-corrected luminosity density $L_{1.4\,\mathrm{GHz}}$, such that:

$$q = \log_{10}\left(\frac{L_{\mathrm{dust}}/3.75\times10^{12}}{L_{1.4\,GHz}}\right). \quad (2)$$

Here 3.75×10^{12} is the frequency corresponding to 80 μm, making q dimensionless. This is equivalent to the definitions given by Helou et al. (1985); Bell (2003) and Ivison et al. (2010b), who quote the logarithmic ratio in terms of flux densities rather than luminosities. In *H*-ATLAS our five bands of far-infrared observations sample wavelengths near (and long-ward of) the peak of the dust SED for local galaxies. Since, as discussed in section 3.1.2, our integrated dust luminosity estimates are not currently accurate enough to probe the small variations in q found by Ivison et al. (2010a), here we focus on the monochromatic equivalents, q_λ, such that:

$$q_\lambda = \log_{10}\left(\frac{L_\lambda}{L_{1.4\,\mathrm{GHz}}}\right), \quad (3)$$

where λ can be any of the PACS/SPIRE wavelengths, e.g. q_{250}. We calculate errors on q_λ by propagating the errors from the input flux densities and k_λ (though the latter source of error is typically small except for the $T < 20$ K sources at 100/160 μm; see section 3.1.3 and appendix A for details).

Since only a small proportion (140/10,387) of the sources in our sample have $> 5\sigma$ detections at 1.4 GHz, we also calculate stacked q_λ for all galaxies in our 250 μm-selected sample. Following Bourne et al. (2011), we derive stacked q_λ for our 250 μm-selected sample by calculating the median k-corrected flux density in each PACS/SPIRE band, then dividing by the median stacked k-corrected 1.4 GHz flux density, according to equation 3. We use median stacking since this method is more resistant to the effects of outliers (due to e.g. residual AGN contamination) in the individual flux density estimates than using the mean. We note that we stack on the k-corrected PACS/SPIRE/FIRST flux densities themselves (i.e. the values which we derive in sections 3.1.3 and 3.2) rather than by producing stacked images (which are more difficult to correctly k-correct). We determine the uncertainties associated with each median stacked flux density by bootstrapping based on 1000 re-samples of the values in each stack; our simulations show that this non-parametric method gives excellent agreement with results obtained using the median statistics method from Gott et al. (2001) used by Bourne et al. (2011), and that it accounts naturally for the uncertainties on the individual values.

3.4 Summary of sample selection

Our study is based on 13,084 galaxies with a signal to noise ratio > 5 at 250 μm, reliable ($R > 0.80$) counterparts in the Smith et al. (2011) likelihood ratio analysis, and spectroscopic redshifts $0.00 < z_{\rm spec} < 0.50$. After removing sources with isophotal semi-major axes > 10 arc sec, 11,389 sources remain, of which 10,437 have good fits to our isothermal model (i.e. they have reduced $\chi^2 < 2.0$). As we will discuss in section 4.1 below, we also remove an additional 50 sources that we classify as AGN, leaving a sample of 10,387 galaxies on which our results are based.

4 RESULTS

4.1 The monochromatic FIRC and its redshift dependence

Before searching for the presence of a correlation between the far-infrared and radio emission of the galaxies in our sample, we must first account for the potential presence of radio-loud AGN; these sources are likely to have excess emission at 1.4 GHz and may bias our estimates of q_λ to lower values. Among the radio sources detected at $> 5\sigma$, we identify those likely to be dominated by powerful AGN rather than star formation using a method similar to that in Hardcastle et al. (2013).[5] This method – which enables us to specify a threshold in q_{250} to identify AGN-dominated sources – was originally based on classifying FIRST-detected radio sources as star-forming or AGN using their optical spectra, and comparing the classifications with q_{250}.

We identify 50 sources which have $q_{250} < 1.2$ as AGN (black triangles in figure 5), and disregard them from what follows.[6] In contrast to a more traditional approach to dealing with AGN contamination, such as removing all sources with the highest radio luminosities (e.g. Mauch & Sadler 2007; Jarvis et al. 2010; Lemaux et al. 2013), this method allows us to keep the most luminous star-forming galaxies in our 250 μm-selected sample, and removes obvious powerful AGN with lower radio luminosities (indicated by the black triangles in figures 2, 4 and 5).

While this method has been shown to identify the most obvious powerful AGN, less obvious low-luminosity AGN are harder to identify, such as those that are not detected at $> 5\sigma$ in the FIRST data, or inefficient AGN which may not have been apparent in the optical spectra used in Hardcastle et al. (2013) when generating the q_{250} criterion (though the latter tend to be "red and dead", and so they are unlikely to meet our 250 μm selection criterion). As a result, though our 250 μm-selection should ensure that our sample is dominated by star-forming galaxies (and the fact that < 1 per cent of our sample are flagged as obvious AGN reflects this) it is possible – or even likely – that some low-luminosity AGN are present. Though the influence of low-luminosity AGN is likely to be strongest on the individual data points (due to our use of median stacked flux densities for calculating q_λ, which should be resistant to moderate levels of AGN contamination), it is still possible that a fraction of the 250 μm sources in our sample harbour AGN which may enhance the average radio luminosity at a lower level. The effect of such an AGN contribution would be to bias our q_λ estimate to lower values, and it is a potential effect that we must bear in mind in what follows. Though removing the 50 sources with $q_{250} < 1.2$ from our stacks has negligible impact upon the results, these represent a sizeable fraction of the 5σ FIRST detected sources (~ 32 per cent), higlighting the importance of our stacking analysis.

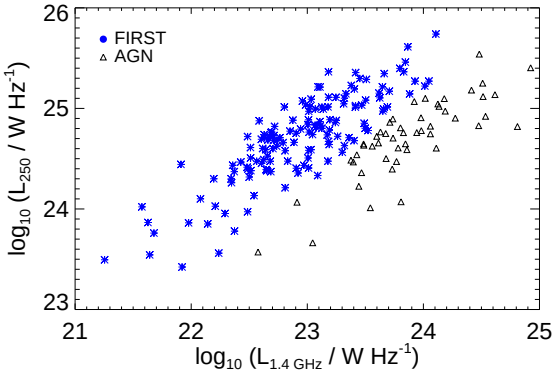

Figure 5. The relationship between $L_{1.4\,\rm GHz}$ and L_{250} for the star-forming galaxies in our sample detected at $> 5\sigma$ at 1.4 GHz (in blue). AGN identified using a method based on that in Hardcastle et al. (2013) are indicated by the black triangles.

In figure 5 we show L_{250} as a function of $L_{1.4\,\rm GHz}$ for the 1.4 GHz detected sources; we observe a strong correlation between the radio and far-infrared, consistent with previous studies (e.g. Garn & Alexander 2009; Garn et al. 2009; Bourne et al. 2011; Ivison et al. 2010a,b; Jarvis et al. 2010), and the sources that we identify as AGN are clearly offset to higher $L_{1.4\,\rm GHz}$, as we would expect.

In the top panel of figure 6, we parameterise the sources in figure 5 using equation 3, and show the 250 μm far-infrared–radio correlation parameter q_{250} as a function of redshift, with the best estimate from Jarvis et al. (2010) overlaid as the dashed horizontal light blue line. Though the individual monochromatic q_{250} for the $> 5\sigma$ 1.4 GHz detected sources show good agreement with the best fit from Jarvis et al. (2010), our stacked estimates in bins of redshift (shown as the green points with error bars) are offset to higher q_{250}. That our stacked values are higher than those for the individual detections is likely a result of the fact that we are determining q_{250} statistically for the full 250 μm galaxy population. The median 1.4 GHz flux density of our sample is around 150 μJy, making the average 250 μm selected galaxy detectable only in the most sensitive radio data. The median stacked q_{250} that we observe ($q_{250} \approx 2.61$) is larger than the value found by Ivison et al. (2010b) using a 250 μm-selected sample of 22 BLAST sources ($q_{250} = 2.18 \pm 0.28$), though the values are consistent within $\sim 1.5\sigma$.

The stacked q_{250} values shown in the top panel of Figure 6 reveal no evidence for evolution with redshift, with the dearth of detected sources at high q_{250} due to the relative lack of sensitivity of FIRST compared to our *Herschel* data; we only detect the brightest 1.4 GHz sources in the FIRST data, and this is reflected by the stacks being offset to higher q_λ than the 1.4 GHz detections. This result – average stacked q_λ being larger than the individually detected data points – highlights the benefits of using a stacking analysis to probe the general population rather than focusing solely on the brightest radio continuum sources in the distribution; we shall return to this offset in the next section.

As well as searching for evolution in q_λ with redshift, in the

[5] See also Condon et al. (1991); Sanders & Mirabel (1996); Yun et al. (2001); Verma et al. (2002).

[6] The potential downside of this approach is that we may miss outliers in the parameter of interest, however previous work on complete samples suggests that we expect very few of these, and our median stacking provides a degree of resistance to the impact of this effect.

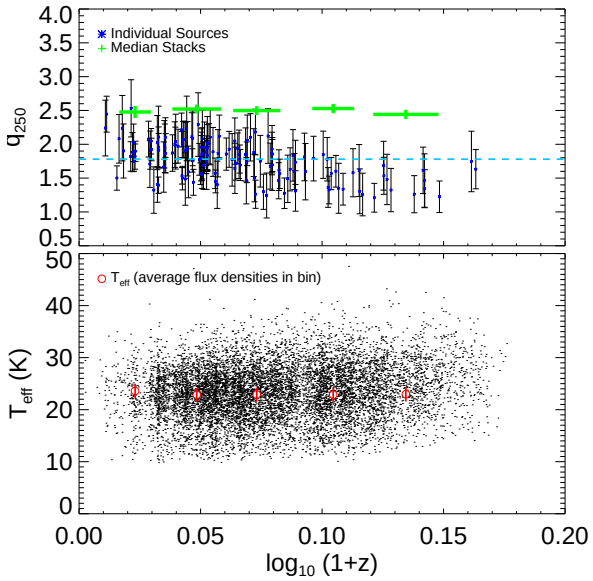

Figure 6. Top: The redshift dependence of the 250 μm monochromatic far-infrared–radio correlation. $> 5\,\sigma$ FIRST sources are shown in blue, with black error bars derived from propagating through the errors on the input luminosities (L_{250} and $L_{1.4\,\mathrm{GHz}}$) and accounting for the uncertainties on the k-corrections. The median stacked q_{250} values for all 250 μm sources in bins of redshift are shown as the green error bars, with the vertical error bars derived by bootstrapping, re-sampling each bin 1000 times. The blue horizontal dashed line indicates the best-fit q_{250} from Jarvis et al. (2010). **Bottom:** T_{eff} versus spectroscopic redshift for the individual sources in our sample (black points) and for the median-stacked flux densities in each redshift bin (red circles with error bars).

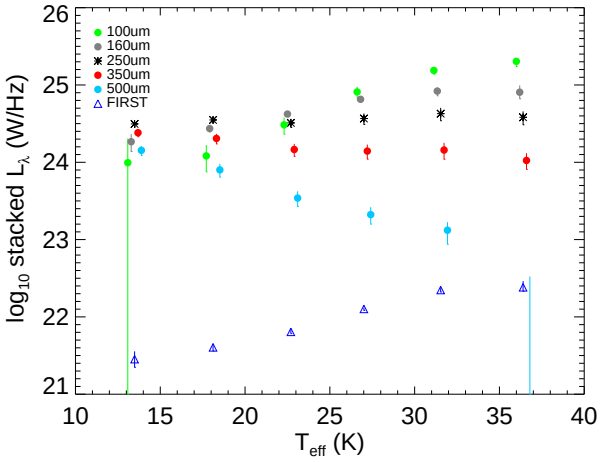

Figure 7. The median-stacked monochromatic luminosity density in the PACS/SPIRE bands (in green, grey, black, red and light blue, from 100-500 μm, respectively), and the FIRST data at 1.4 GHz (in blue). The errors have been estimated based on bootstrapping 1000 resamples of the data, and added in quadrature with the uncertainties on the k-corrections as a function of temperature. The median-stacked monochromatic luminosity density at 500 μm in the hottest bin is negative (though not statistically significant), and thus only the upper part of the error bar is visible on the logarithmic vertical axis. The individual PACS/SPIRE data points have been slightly offset at intervals of 0.2 K in the abscissa to prevent the error bars from obscuring one another. There are 641, 1973, 3872, 2912, 843 and 146 galaxies in each bin, with the numbers listed in order of increasing temperature.

lower panel of figure 6 we search for variation in temperature with redshift. Spearman's rank tests reveal no significant evidence for correlation between temperature and redshift for the individual galaxies (black points; the asymmetric error bars on T_{eff} are not shown for clarity). In addition, if we fit isothermal models to the stacked k-corrected flux densities in bins of redshift, we find that the best-fit temperature in each bin is consistent with no evolution (red circles with error bars in the lower panel of figure 6).

4.2 The temperature dependence of the FIRC in *H*-ATLAS

Before analysing the q_λ, we first show the median-stacked monochromatic luminosity densities in Figure 7, in bins of temperature. The PACS and SPIRE values are shown with error bars indicating the sum in quadrature of the bootstrapped errors on the median fluxes and the uncertainties on k_λ, while the 1.4 GHz values (blue triangles) include only bootstrapped errors (though as we discussed in section 3.2, 100 Monte-Carlo realisations of the 1.4 GHz k-corrections revealed that this source of uncertainty is smaller than the bootstrapped errors on the stacked values).

Interestingly, we find that the stacked k-corrected 1.4 GHz luminosity densities (blue triangles in figure 7) reveal a clear increase with the effective temperature of the dust SED (the increase is around an order of magnitude between the coldest and warmest bins of our sample). This is indicative of warmer galaxies hosting larger levels of star formation, as expected based on the FIRC combined with the far-infrared luminosity–temperature ("L–T") relation found by several previous studies (e.g. Chapman et al. 2003; Hwang et al. 2010; Smith et al. 2013). We observe this relationship at radio wavelengths for the first time. The lack of temperature evolution in our sample (highlighted in the lower panel of figure 6) suggests that this trend, the radio-luminosity–temperature relation, is not simply the result of redshift/luminosity effects.

Figure 8 shows the k-corrected stacked flux densities (in black) for the same six temperature bins shown in figure 7, overlaid (in red) with isothermal models corresponding to the median temperature of the galaxies in that bin. These panels highlight how well the stacked flux densities in figure 8 are described by the isothermal model that we use to estimate temperatures.

In figure 9 we show the variation of the monochromatic FIRC parameters as a function of temperature (q_{100}, q_{160}, q_{250}, q_{350}, q_{500} from top to bottom, respectively). Whilst in every panel we require a $\geq 5\sigma$ detection at 250 μm, we also require a $\geq 5\sigma$ detection in the particular band shown for an individual source to be included. We display the sources detected at $\geq 5\sigma$ in FIRST as the blue crosses, and overlay the stacked q_λ in bins of temperature as green error bars, derived as discussed in section 3.3, and based on the median stacked luminosity densities shown in figure 7. As in figure 6, we find that if we consider only the 250 μm sources which are detected at 1.4 GHz, we recover values of q_λ offset from the values stacked across the whole 250 μm selected population (shown in green in figure 9).

At the PACS wavelengths, the stacked values reveal that q_{100} shows little evidence for variation as a function of effective dust temperature, however as we move to progressively longer wavelengths q_{160}, q_{250}, q_{350} and q_{500} show increasingly strong negative correlations with the effective temperature of the far-IR SED. A previous study of the temperature dependence of the FIRC (Ivison et al. 2010a) found evidence for weak negative correlation between the integrated q and dust temperature, concentrating on a 250 μm-selected sample of 128 galaxies with a mean redshift ~ 1.

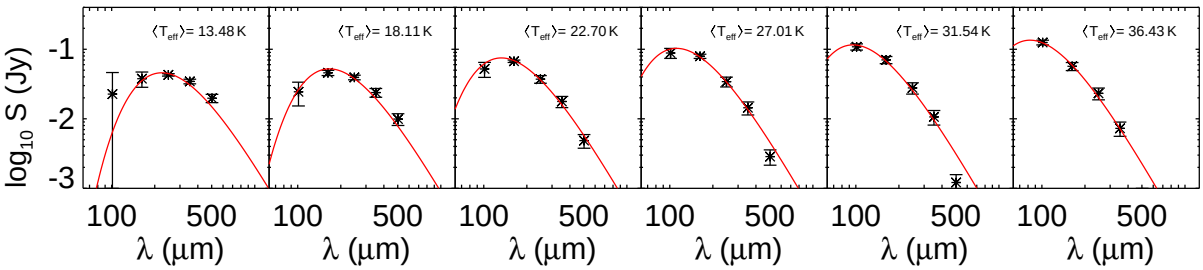

Figure 8. The k-corrected stacked flux densities (black asterisks with error bars) in each of the six temperature bins, overlaid with an isothermal dust SED (in red). The median temperature of the individual galaxies in each bin is used to define the isothermal model, and is displayed in the top right corner.

The Ivison et al. (2010a) 250 μm selection at $z \sim 1$ corresponds to selection at $\sim 100-160$ μm (near the peak of the dust SED) in the rest frame, where our monochromatic values show broadly consistent behaviour. We are currently unable to probe integrated q using the *H*-ATLAS data set, though the fact that q in Ivison et al. (2010a) and q_{100}/q_{160} in this study are approximately temperature independent offers some encouragement for the use of $L_{\rm dust}$ as an SFR indicator in certain situations (though see also da Cunha et al. 2012; Smith et al. 2012; Hayward et al. 2014; Rowlands et al. 2014).

We must also consider the possible influence of contamination in the 250 μm cross-identifications upon our results. Bourne et al. (2014) suggest that the 250 μm-SDSS cross-identification analysis in Smith et al. (2011) may have overestimated the number of reliable associations for the coldest sources in *H*-ATLAS with $T < 15$ K. However, the trends that we see in figure 9 all remain unchanged even in the implausible extreme scenario in which erroneous cross-IDs dominate the sources in the coldest bin, therefore our results and conclusions are robust to these effects.

4.3 Discussion

If we assume a simple two-component model of the dust SED, similar to that proposed by e.g. Charlot & Fall (2000) and implemented in MAGPHYS (da Cunha et al. 2008), we expect the 100 μm PACS observations to sample emission associated with the warm stellar birth cloud (BC) dust component of a galaxy, and to show a strong correlation with the most recent burst of star formation due to heating dominated by short-lived OB stars. In contrast, we expect that the longer wavelength observations should be dominated by emission from colder dust in the ambient interstellar medium (ISM), perhaps heated by more evolved stars and more weakly correlated with recent star formation. The influence of the ISM on the FIRC is highlighted by Vlahakis et al. (2007), who attributed the larger variation in the FIRC at 850 μm compared to 60 μm to the influence of a varying cold dust component. In the ISM+BC scenario, it is relatively straightforward for a comparatively low-mass component of warm dust in the BC to become more luminous than the cooler, more massive, ISM component at 250 μm due to the strong temperature dependence of [modified] black body radiation. Furthermore, black body physics implies that the shorter wavelengths (i.e. the BC) fade more rapidly after the truncation of star formation than the longer wavelengths as the gas cools. The exact temperature dependence of the monochromatic q_λ may also be affected by differing decay times for the dust SED and the synchrotron energy density following the truncation of star formation, a possibility investigated in detail by Lacki et al. (2010) and Lacki & Thompson (2010), to which we refer the reader for further details.

In this simple two-component scenario galaxies can meet our 250 μm selection criterion by having an SED dominated by a low-mass, warm BC component, through having a dominant high-mass cold ISM component, or some mix of the two as we move from the hottest to the coldest SEDs in our sample. An estimate of the proportion of the total dust luminosity contributed by the ISM – "f_μ" – is produced by the MAGPHYS SED fitting for *H*-ATLAS galaxies in Smith et al. (2012). Though the individual f_μ estimates have large uncertainties, we determine the median f_μ in temperature bins, and find weak evidence for decreasing f_μ with increasing effective temperature. This suggests that the BC are more dominant at warmer temperatures (as we would expect), but the weak trend hints that the true situation is likely more complicated than the simple two component model, and that the temperature information is inadequate to determine the relative mix of BC and ISM emission in galaxies on its own.

The physical difference between the two extremes in temperature for this simple model, and the 250 μm selection, may be the dominant forces in the variation of q_{500} (since the 500 μm luminosity varies much more than the luminosity at 1.4 GHz across our temperature range). In contrast, the 100 μm data are generally dominated by dust heated in the most recent burst of star formation, due to the much stronger dependence of 100 μm luminosity on temperature than on dust mass, and so less variation in q_{100} might be expected if we assume that the 1.4 GHz emission is also related to the most recent burst. This highlights that studies of the FIRC – or investigations assuming a constant FIRC – must be wary of temperature effects if wavelengths away from the peak of the dust SED are used.

Though we account for the presence of obvious AGN contamination using the method of Hardcastle et al. (2013), it is possible that our sample contains residual low-level AGN contamination, which has the potential to bias our results to lower q_λ. In an attempt to simulate the influence of residual AGN-contamination on our results, we perform a simple test; we arbitrarily assume that the 1.4 GHz flux density of a random 15 per cent of our sample is dominated by AGN. We "correct" these values by artificially replacing them with values drawn from a random distribution with a median of zero and standard deviation equal to the local RMS flux density from the FIRST maps appropriate for each source (i.e. with values consistent with zero). Repeating our analysis using these artifical "AGN-subtracted" values results in our FIRC estimates shown in figure 6 and 9 being offset to larger q_λ by ~ 0.1 dex.[7] We conclude

[7] Performing the same simulation, but instead assuming the extreme case in which 50 per cent of our sample has 1.4 GHz flux density entirely due to AGN, and replacing those values in the same way (i.e. making them consistent with zero), alters our results in figures 6 and 9 to larger q_λ by ~ 0.3 dex.

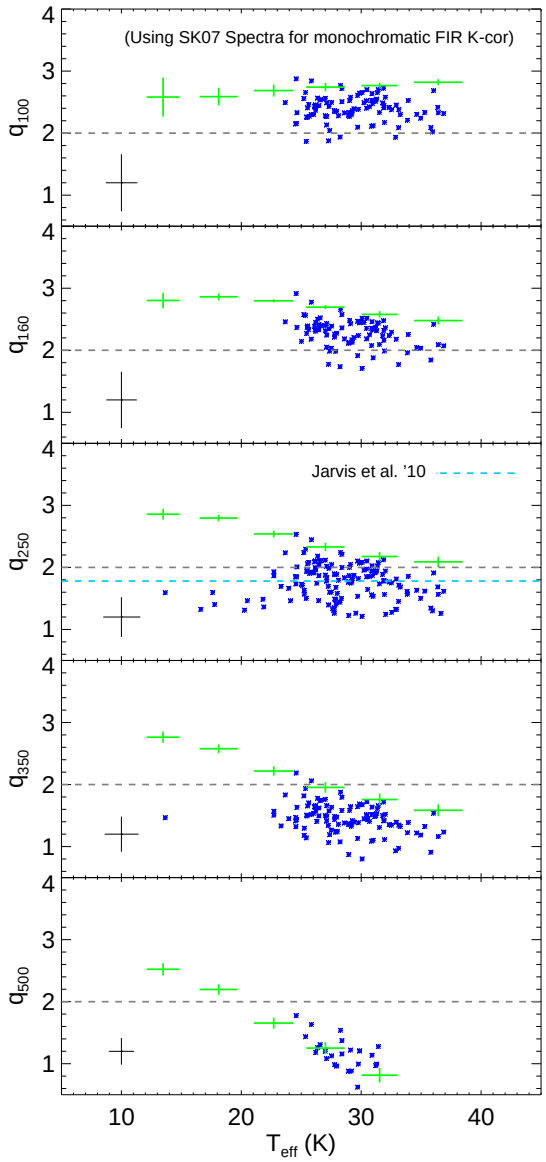

Figure 9. Variation of the monochromatic FIRCs as a function of effective temperature. In addition to the initial catalogue selection (i.e. $\geq 5\sigma$ at 250 μm, $\geq 5\sigma$ at 1.4 GHz), we require a minimum $5\,\sigma$ detection in the relevant band for the individual monochromatic q_λ to be plotted; this is reflected in the lower number of blue points in the q_{500} panel compared with the other bands. The stacked q_λ are shown as the green error bars, while the horizontal grey dashed lines indicate $q_\lambda = 2$, to guide the eye. The stacked q_{500} in the warmest temperature bin is negative (as discussed in the caption to figure 7) and so not displayed here. The median error uncertainty for the individually-detected sources is shown by the black error bar in the lower left corner of each panel.

that though it is possible that residual AGN exert some influence on the results of our stacking analyses, this influence is likely to be small.

Our results highlight potential problems with using single-band dust luminosities to estimate star formation rates in galaxies, due to the varying influence of the ISM on the total dust luminosity. It may be possible to mitigate these effects by making reasonable assumptions about the SED, or by sampling wavelengths near the temperature-dependent peak of the thermal dust emission. These are important considerations given, for example, the very different sensitivity at 450 and 850 μm of SCUBA-2, and since the 850 μm channel samples the 250 μm rest-frame emission of galaxies at $z \approx 2.4$ and 160 μm rest-frame emission at $z \gtrsim 5.3$. Deriving monochromatic luminosities in this way may be less susceptible to the effects of assuming an inappropriate dust SED than using the integrated dust luminosity as a star formation rate indicator.

5 CONCLUSIONS

We have used a 250 μm-selected sample of 10,387 low-redshift ($z_{\rm spec} < 0.50$) galaxies from the *H*-ATLAS survey, with isophotal major axes < 10 arc sec and spectroscopic redshifts, plus aperture photometry at 1.4 GHz based on data from the FIRST survey to probe the far-infrared–radio correlation (FIRC). In order to representatively probe the monochromatic FIRC, rather than focussing only on the small sub-set of sources detected at 1.4 GHz, we measure aperture flux densities directly from the FIRST images for every galaxy. This enables us to determine the FIRC by median stacking the flux densities for galaxies in our sample as a function of parameters of interest, as well as considering the individual galaxies with formal detections.

We find that the monochromatic q_{250} that we determine for individual galaxies (i.e. those that are detected at $> 5\sigma$ in both the *Herschel* and FIRST observations) are consistent with expectations based on previous studies (e.g. Ivison et al. 2010b; Jarvis et al. 2010). In contrast, the stacked q_{250} for our whole 250 μm selected sample are offset to higher values than those found in Jarvis et al. (2010), highlighting the importance of stacking techniques applied to large samples of sources. Though it is possible that some fraction of our sample could contain low-level AGN, the median stacking that we use, coupled with the fact that our results are offset to higher q_λ (i.e. *lower* 1.4 GHz luminosities than the detections in our sample, or that of Jarvis et al. 2010), as well as our simulations (which suggest that the influence of residual AGN contamination – if it is present – is likely to be small), all offer encouragement in this regard.

Using the *H*-ATLAS catalogue and our FIRST flux densities we find no evidence for redshift evolution of the FIRC as probed by the k-corrected monochromatic 250 μm luminosity density. This lack of obvious evolution is in agreement with several previous studies (e.g. Boyle et al. 2007; Garn & Alexander 2009; Garn et al. 2009; Jarvis et al. 2010; Ivison et al. 2010a; Bourne et al. 2011), though we show this with a sample size unprecedented at these redshifts for the first time.

In order to probe the temperature dependence of the monochromatic FIRC we began by determining stacked FIRST luminosities in temperature bins, revealing that the 1.4 GHz luminosity increases as a function of the effective dust temperature. This represents a radio continuum version of the far-infrared Luminosity-Temperature ("L-T") relations discussed in several previous studies (e.g. Chapman et al. 2003; Hwang et al. 2010; Smith et al. 2013; Symeonidis et al. 2013). This cannot be simply attributed to redshift or selection effects for two main reasons. Firstly, unlike the 1.4 GHz luminosity, we find that the effective dust temperature of the stacked k-corrected PACS/SPIRE SED in bins of redshift is constant. Secondly, our temperature estimates (along with the results of Symeonidis et al. 2011) suggest that our 250 μm-selection includes galaxies with the vast majority of dust temperatures at these redshifts (though we note that we may miss galaxies with the very hottest temperatures > 50K, or non-AGN

radio-selected IR sources with low q_λ; it is unclear how many of these exist at $z < 0.5$).

We use our stacked PACS/SPIRE/FIRST flux densities to show that the monochromatic FIRCs, q_λ, show varying temperature dependence. We find that q_λ is roughly constant when sampling near the peak of the dust SED (i.e. at 100 and 160 μm), and that it shows progressively stronger inverse correlation with temperature as we move to the SPIRE observations at 250, 350 and 500 μm. We suggest that monochromatic far-IR data may be reliably used as star formation rate indicators in particular situations, such as when the observations sample wavelengths around 100 μm in the rest-frame. At these wavelengths, the fact that our results show a temperature independent FIRC suggests that the far-IR SED is dominated by dust heated in the most recent burst of star formation (i.e. the stellar birth cloud component in the two model of Charlot & Fall 2000) whatever the effective temperature of the far-IR SED.

The far-IR temperature/colour dependence of the FIRC is likely to be of critical importance for future investigations, given the impending explosion of Square Kilometre Array pathfinder and precursor radio continuum surveys from ASKAP (Norris et al. 2011), LOFAR (Röttgering et al. 2011), MeerKAT (Jarvis 2012), and the Jansky Very Large Array (JVLA). Radio observations will be crucial in the future, since they will not only be sufficiently sensitive to detect the entire $z < 0.5$ star-forming galaxy population, they may also provide a more reliable tracer of a galaxy's star formation rate than observations sampling long far-IR wavelengths ($> 250\,\mu$m). The results in this paper and the data from these facilities are likely to be critical for future studies of star-forming galaxies.

ACKNOWLEDGMENTS

The authors would like to sincerely thank the anonymous reviewer for their thoughtful report which improved this paper. DJBS, MJJ, MV, NM and MP also wish to thank the National Research Foundation of South Africa for financial assistance. The authors would like to thank Chris Hayward, Dominic Benford, Rob Ivison, Michal Michałowski and Paul van der Werf for useful discussions. NB acknowledges funding from the EC FP7 SPACE project ASTRODEEP (Ref. no. 312725). EI acknowledges funding from CONICYT/FONDECYT postdoctoral project N°:3130504. The *Herschel*-ATLAS is a project with *Herschel*, which is an ESA space observatory with science instruments provided by European-led Principal Investigator consortia and important with participation from NASA. The *H*-ATLAS website is `http://www.h-atlas.org/`. GAMA is a joint European-Australasian project based around a spectroscopic campaign using the Anglo-Australian Telescope. The GAMA input catalogue is based on data taken from the Sloan Digital Sky Survey and the UKIRT Infrared Deep Sky Survey. GAMA is funded by the STFC (UK), the ARC (Australia), the AAO, and the participating institutions. The GAMA website is http://www.gama-survey.org/. This work used data from the SDSS DR7. Funding for the SDSS and SDSS-II has been provided by the Alfred P. Sloan Foundation, the Participating Institutions, The National Science Foundation, the U.S. Department of Energy, the National Aeronautics and Space Administration, the Japanese Monbukagakusho, the Max Planck Society and the Higher Education Funding Council for England.

REFERENCES

Appleton P. N. et al., 2004, ApJS, 154, 147
Baldry I. K. et al., 2010, MNRAS, 404, 86
Becker R. H., White R. L., Helfand D. J., 1995, ApJ, 450, 559
Bell E. F., 2003, ApJ, 586, 794
Bendo G. J. et al., 2012, MNRAS, 419, 1833
Bourne N., Dunne L., Ivison R. J., Maddox S. J., Dickinson M., Frayer D. T., 2011, MNRAS, 410, 1155
Bourne N. et al., 2014, ArXiv e-prints
Boyle B. J., Cornwell T. J., Middelberg E., Norris R. P., Appleton P. N., Smail I., 2007, MNRAS, 376, 1182
Calzetti D. et al., 2010, ApJ, 714, 1256
Chapman S. C., Helou G., Lewis G. F., Dale D. A., 2003, ApJ, 588, 186
Charlot S., Fall S. M., 2000, ApJ, 539, 718
Cluver M. E. et al., 2014, ApJ, 782, 90
Condon J. J., 1992, ARA&A, 30, 575
Condon J. J., Cotton W. D., Greisen E. W., Yin Q. F., Perley R. A., Taylor G. B., Broderick J. J., 1998, AJ, 115, 1693
Condon J. J., Huang Z.-P., Yin Q. F., Thuan T. X., 1991, ApJ, 378, 65
da Cunha E., Charlot S., Dunne L., Smith D., Rowlands K., 2012, in IAU Symposium, Vol. 284, IAU Symposium, Tuffs R. J., Popescu C. C., eds., pp. 292–296
da Cunha E., Charlot S., Elbaz D., 2008, MNRAS, 388, 1595
Dale D. A. et al., 2012, ApJ, 745, 95
de Jong T., Clegg P. E., Rowan-Robinson M., Soifer B. T., Habing H. J., Houck J. R., Aumann H. H., Raimond E., 1984, ApJ, 278, L67
de Jong T., Klein U., Wielebinski R., Wunderlich E., 1985, A&A, 147, L6
Draine B. T. et al., 2007, ApJ, 663, 866
Driver S. P. et al., 2011, MNRAS, 413, 971
Dunne L., Eales S., Edmunds M., Ivison R., Alexander P., Clements D. L., 2000, MNRAS, 315, 115
Dunne L., Eales S. A., 2001, MNRAS, 327, 697
Dunne L. et al., 2011, MNRAS, 417, 1510
Eales S. et al., 2010, PASP, 122, 499
Frayer D. T. et al., 2006, AJ, 131, 250
Garn T., Alexander P., 2009, MNRAS, 394, 105
Garn T., Green D. A., Riley J. M., Alexander P., 2009, MNRAS, 397, 1101
Garrett M. A., 2002, A&A, 384, L19
Gott, III J. R., Vogeley M. S., Podariu S., Ratra B., 2001, ApJ, 549, 1
Griffin M. J. et al., 2010, A&A, 518, L3
Hardcastle M. J. et al., 2013, MNRAS, 429, 2407
Hayward C. C. et al., 2014, ArXiv e-prints
Helou G., Soifer B. T., Rowan-Robinson M., 1985, ApJ, 298, L7
Helou G., Walker D. W., eds., 1988, Infrared astronomical satellite (IRAS) catalogs and atlases. Volume 7: The small scale structure catalog, Vol. 7
Hwang H. S. et al., 2010, MNRAS, 409, 75
Ibar E. et al., 2008, MNRAS, 386, 953
Ibar E. et al., 2010, MNRAS, 409, 38
Ivison R. J. et al., 2010a, MNRAS, 402, 245
Ivison R. J. et al., 2010b, A&A, 518, L31
Jarvis M. J., 2012, African Skies, 16, 44
Jarvis M. J. et al., 2010, MNRAS, 409, 92
Kennicutt R. C., Evans N. J., 2012, ARA&A, 50, 531
Kennicutt, Jr. R. C., 1998, ARA&A, 36, 189

Lacki B. C., Thompson T. A., 2010, ApJ, 717, 196
Lacki B. C., Thompson T. A., Quataert E., 2010, ApJ, 717, 1
Lemaux B. C. et al., 2013, ArXiv e-prints
Massardi M., Bonaldi A., Negrello M., Ricciardi S., Raccanelli A., de Zotti G., 2010, MNRAS, 404, 532
Mauch T., Klöckner H.-R., Rawlings S., Jarvis M., Hardcastle M. J., Obreschkow D., Saikia D. J., Thompson M. A., 2013, MNRAS, 435, 650
Mauch T., Sadler E. M., 2007, MNRAS, 375, 931
Michałowski M., Hjorth J., Watson D., 2010, A&A, 514, A67
Moshir M., Kopman G., Conrow T. A. O., 1992, IRAS Faint Source Survey, Explanatory supplement version 2
Murphy E. J., Chary R.-R., Alexander D. M., Dickinson M., Magnelli B., Morrison G., Pope A., Teplitz H. I., 2009, ApJ, 698, 1380
Neugebauer G. et al., 1984, ApJ, 278, L1
Norris R. P. et al., 2011, PASA, 28, 215
Pascale E. et al., 2011, MNRAS, 415, 911
Pilbratt G. L. et al., 2010, A&A, 518, L1
Planck Collaboration et al., 2011, A&A, 536, A25
Poglitsch A. et al., 2010, A&A, 518, L2
Popescu C. C., Tuffs R. J., Völk H. J., Pierini D., Madore B. F., 2002, ApJ, 567, 221
Rigby E. E. et al., 2011, MNRAS, 415, 2336
Robotham A. et al., 2010, PASA, 27, 76
Röttgering H. et al., 2011, Journal of Astrophysics and Astronomy, 32, 557
Rowlands K. et al., 2014, MNRAS, 441, 1017
Sanders D. B., Mirabel I. F., 1996, ARA&A, 34, 749
Sargent M. T. et al., 2010, ApJ, 714, L190
Sauvage M., Thuan T. X., 1992, ApJ, 396, L69
Seymour N., Huynh M., Dwelly T., Symeonidis M., Hopkins A., McHardy I. M., Page M. J., Rieke G., 2009, MNRAS, 398, 1573
Siebenmorgen R., Krügel E., 2007, A&A, 461, 445
Smith D. J. B. et al., 2012, MNRAS, 427, 703
Smith D. J. B. et al., 2011, MNRAS, 416, 857
Smith D. J. B. et al., 2013, MNRAS, 436, 2435
Symeonidis M., Page M. J., Seymour N., 2011, MNRAS, 411, 983
Symeonidis M. et al., 2013, MNRAS, 431, 2317
van der Kruit P. C., 1971, A&A, 15, 110
Verma A., Rowan-Robinson M., McMahon R., Efstathiou A., 2002, MNRAS, 335, 574
Vlahakis C., Dunne L., Eales S., 2005, MNRAS, 364, 1253
Vlahakis C., Eales S., Dunne L., 2007, MNRAS, 379, 1042
Wang L., Rowan-Robinson M., 2009, MNRAS, 398, 109
Wilman R. J., Jarvis M. J., Mauch T., Rawlings S., Hickey S., 2010, MNRAS, 405, 447
Wilman R. J. et al., 2008, MNRAS, 388, 1335
Windhorst R. A., 2003, New Annual Reviews, 47, 357
Wright E. L. et al., 2010, AJ, 140, 1868
Yang M., Greve T. R., Dowell C. D., Borys C., 2007, ApJ, 660, 1198
York D. G. et al., 2000, AJ, 120, 1579
Yun M. S., Reddy N. A., Condon J. J., 2001, ApJ, 554, 803

APPENDIX A: MORE SED FITS AND K-CORRECTIONS

A1 Integrated dust luminosities

Since isothermal models do not include any mid-IR contribution to the total dust luminosity from warmer dust components, such as hot very small grains (e.g. Yang et al. 2007), we have used three alternative methods to try and quantify the likely impact that our choice of SED will have on our derived dust luminosities/k-corrections. The additional methods we use to calculate $L_{\rm dust}$ are described below:

- As discussed in section 3.1.3, we fit our PACS and SPIRE data using the panchromatic SED templates from Siebenmorgen & Krügel (2007, hereafter SK07). Though Smith et al. (2012) found that these templates did not reproduce the optical/near-IR properties of *H*-ATLAS galaxies, the SK07 templates are the only set of available multi-component templates that include models cold enough to describe the far-IR SEDs of sources with $T_{\rm eff} < 15\,{\rm K}$ that we find in *H*-ATLAS. We derive the best fits based on these models using the PACS/SPIRE data alone.
- We also use results based on MAGPHYS (da Cunha et al. 2008, hereafter DC08); a panchromatic SED fitting code which assumes consistency between the energy absorbed by dust (using a two-component obscuration model from Charlot & Fall 2000), and the energy reradiated in the far-infrared. MAGPHYS produces best-fit and median-likelihood estimates of dust luminosity in the same way as our isothermal fitting, and the application of MAGPHYS to the *H*-ATLAS data set is described in great detail in Smith et al. (2012, hereafter S12). We note that the coldest dust temperature component included in the DC08 dust library is 15 K, meaning that MAGPHYS is unable to accurately reproduce the dust SEDs of the minority of sources colder than this using the standard priors. We also note that the temperatures of the two dust SED components included in MAGPHYS do not, in general, map onto the effective temperatures that we derive for our sample based on the isothermal model.
- We also derived estimates of $L_{\rm dust}$ using the DC08 far-IR SED template library without using the optical/near-IR data, i.e. without using the energy balance criterion imposed, deriving $L_{\rm dust}$ estimates in the same way as for the SK07 models, above. We refer to these values as the DC08 results in what follows.

We find that there are temperature-dependent offsets between the integrated dust luminosities derived using each of these methods; "correcting" the isothermal values to total integrated dust luminosities is highly temperature/model dependent. For example, we are unable to assume a simple correction factor to convert the isothermal dust luminosity to agree with the MAGPHYS estimates, as it is a function of temperature, with significant scatter.

In this investigation we would also like to probe the temperature dependence of the integrated FIRC (i.e. to update and build on the study by Jarvis et al. 2010, in light of the newly-available PACS data, $10\times$ larger areal coverage and additional spectroscopic redshifts). The only previous investigation of this dependence (Ivison et al. 2010a) found variations on the scale of ~ 0.1 dex over the temperature range probed in *H*-ATLAS, but the uncertainties on even the MAGPHYS dust luminosities (due to the variable contribution from the mid-infrared) are larger than this. Furthermore, the differences between the dust luminosities derived using the different SED fits discussed above are compounded by the absence of sensitive mid-infrared data available for our SED fitting at the time of writing (as highlighted by Smith et al. 2012, and dis-

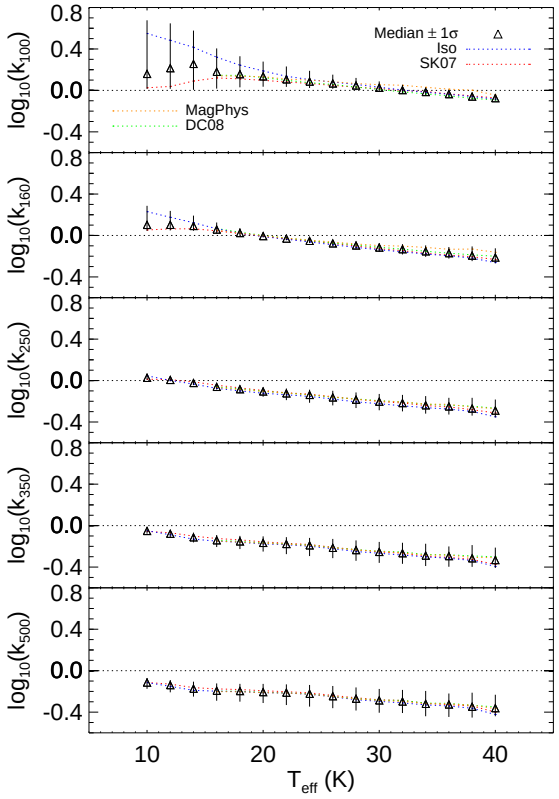

Figure A1. The median k-corrections (k_λ; triangles) at each of the PACS/SPIRE wavelengths as a function of temperature, conservatively averaged over the sets of SED fits, and over redshift. The uncertainty on k_λ as a function of $T_{\rm eff}$ is shown by the error bars, with median values of 25.3, 11.6, 14.3, 18.0 and 21.4 per cent in each of the PACS/SPIRE bands in increasing order of wavelength. The largest uncertainties rise to a factor of ~ 3 on k_{100} at $T_{\rm eff} \approx 10\,{\rm K}$. The coloured dotted lines indicate the median k_λ using each individual set of templates, with the colour-coding indicated in the legends.

cussed in section 3.1.2). As a result, we are unable to address the temperature dependence of the integrated FIRC at this time, and so leave this topic for a future study.

A2 Uncertainties on k-corrections

We generate conservative estimates of the uncertainties on the monochromatic k-corrections by first calculating k_λ for every source using each of the four sets of template SEDs (isothermal, SK07, MAGPHYS and DC08). We then bin our sample by isothermal temperature, and calculate the standard deviation, $\sigma\,(k_\lambda)$, across the bin occupants. In calculating $\sigma\,(k_\lambda)$ for a particular temperature bin, we include the best-fit k_λ to each galaxy derived using each of the aforementioned SED libraries (providing that they have reduced $\chi^2 < 2$).

We suggest that the resulting estimates of $\sigma\,(k_\lambda)$ are likely to be conservative (i.e. over-estimated) for two reasons. Firstly, the range of SEDs in the isothermal, SK07 and DC08 libraries is probably larger than the range of SEDs of star-forming galaxies in *H*-ATLAS, particularly at $\lambda_{\rm obs} < 100\,\mu$m where we use the templates to extrapolate beyond the observational data, and where we know that the isothermal models underestimate the true SED. Secondly, we calculate global values as a function of temperature alone, rather than calculating $\sigma(k_\lambda)$ as a function of redshift (i.e. we do not discriminate between our differing ability to determine temperatures for e.g. $T_{\rm eff} = 20\,{\rm K}$ galaxies at $z = 0.5$ compared to galaxies with the same temperature at $z = 0.05$). Finally, we note that in deriving $\sigma\,(k_\lambda)$, we include four sets of templates above $T_{\rm eff} = 15\,{\rm K}$, while at colder temperatures we include only the isothermal and SK07 templates in the averaging, since the standard MAGPHYS libraries used for the other two sets of fits do not include dust SED components colder than 15 K.

The median $\sigma\,(k_\lambda)$, shown in figure A1, range from ~ 14 per cent at 250 μm (where the dust SED is best-sampled) to ~ 25 per cent at 100μm (at the edge of our far-IR wavelength coverage, and where the different SEDs show most variation), though the uncertainty on k_{100} at the coldest temperatures is rather larger. We propagate the uncertainties shown in figure A1 onto our dust luminosity estimates by adding them in quadrature with the uncertainties on the flux densities in the *H*-ATLAS catalogue; these are then propagated through onto the individual q_λ.

This paper has been typeset from a TEX/ LATEX file prepared by the author.